Supplementary information

S.1 Task specifics

For both the instructed path task and the point-to-point task, the targets were defined by two parameters: the visible radius and the tolerance radius. The visible radius is the radius of the target as it appears on the screen. The tolerance radius defines the tolerance region around the target. In order to 'acquire' a target, the center of the cursor needed to be within the tolerance region around the target. Visually, this sometimes corresponded to the edge of the cursor just touching the edge of the target, and sometimes the cursor being a few pixels within the target. All targets appeared as yellow circles on the screen. The start and end target visible radii ranged from 1.4 to 2.5 cm, and the tolerance radii ranged from 1 to 3.5 cm. The cursor radius ranged from 1 to 1.8 cm. The cursor was a blue circle for brain control trials and as a red circle for arm control trials.

For some sessions, the start target appeared in the center of the workspace. For those trials, the end target was selected from 8 possible locations uniformly spaced on a circle around the start target. The distance from the start target to the end target was 15.2 cm. For other sessions, the start target appeared in 1 of 8 locations uniformly spaced on a circle around the center of the workspace. For those trials, the end target was located on the circle diametrically opposite the start target. The distance from the start target to the end target was 20 cm. For some brain control point-to-point sessions for monkey J, a start target did not appear. At the start of each of those trials, the cursor was automatically placed in the center of the workspace at the same time as the end target appeared.

The instructed paths had a path tolerance radius. This radius defined the maximum distance the center of the cursor could be from any point along the center-line of the path. The path tolerance ranged from 1.6 to 5 cm. The width of the instructed path as it appeared on the screen was 8% of the straight-line distance from the start target to the end target. For a given pair of start and end targets, there were two possible orientations of a single-inflection path (i.e., clockwise and counter-clockwise inflections).

The specific target and task parameters that we used for each experimental session are listed in Table S1.

Table S1: Task types and decoding parameters for every session. Sessions are listed in chronological order. All distances and radii are in cm. [1]a = arm control, b = brain control. [2]pp = point-to-point task, ip = instructed path task. [3]This is the straight-line distance from the center of the start target to the center of the end target. [4]start target display radius, end target display radius. [5]start target tolerance radius, end target tolerance radius, path tolerance radius (if applicable); numbers in parentheses indicate different radii used in the same session. [6]m = modified Kalman filter, s = standard Kalman filter; number in parentheses is p, the dimensionality of the factor analysis model; number after comma is r, the number of decoded kinematic parameters. If multiple decoders were used in a session, the decoder parameters are separated by a semi-colon. [7]a = arm control (monkey J, method 1), o = observation (monkey J, method 2), g = gradual procedure (monkey L).

Session	Monkey	Control type[1]	Task type[2]	Target distance[3]	Cursor radius	Target visible radius[4]	Target tolerance radius[5]	Decoder format[6]	Decoder calibration[7]
1	J	a	ip	15.2	1.5	1.8, 1.4	1, 1.2, (1.6, 1.7)	-	-
2	J	a	pp	15.2	1.8	2, 1.5	2, 1.5, -	-	-
3	J	a	ip	15.2	1.5	1.8, 1.4	1, 1.2, (1.6, 1.7)	-	-
4	J	a	pp	15.2	1.8	2, 1.5	2, 1.5, -	-	-
5	J	a	ip	15.2	1.5	1.8, 18	1, 1.2, (1.6, 1.7)	-	-
6	J	a	pp	15.2	1.8	2, 1.5	2, 1.5, -	-	-
7	J	a	ip	15.2	1.5	1.8, 1.5	1.2, 1.2, (1.6, 1.7)	-	-
8	J	a	pp	15.2	1.8	2, 1.5	2, 1.5, -	-	-
9	J	a	ip	15.2	1.5	1.8, 1.5	1.2, 1.2, (1.6, 1.7)	-	-
10	J	a	pp	15.2	1.8	2, 1.5	2, 1.5, -	-	-
11	J	a	ip	15.2	1.5	1.8, 1.4	1, 1.2, 1.7	-	-
12	J	a	ip	15.2	1.5	1.8, 1.4	1, 1.2, (1.6, 1.7)	-	-
13	J	a	ip	15.2	1.5	1.8, 1.4	1, 1.2, (1.6, 1.7)	-	-
14	J	a	ip	15.2	1.5	1.8, 1.4	1, 1.2, 1.6	-	-
15	J	b	ip	22.7	1.8	1.5, 1.5	2, 2, 3.5		a
16	J	b	pp	15.2	1.8	1.5, 1.5	1.7, 1.7, -	m(1), 6	a
17	J	a	ip	22.7	1.8	1.5, 1.5	2, 2, 3.5	-	-
18	J	a	pp	15.2	1.8	1.5, 1.5	2, 2, -	-	-
19	J	b	ip	22.5	1.8	1.5, 1.5	2, 2, 5	s, 6	a
20	J	b	ip	22.5	1.8	1.5, 1.5	2, 2, 5	s, 6	a
21	J	b	ip	22.5	1.8	1.5, 1.5	2, 2, 5	s, 6	a
22	J	b	ip	22.5	1.8	1.5, 1.5	2, 2, 5	s, 6	a
23	J	b	ip	22.5	1.8	1.5, 1.5	2, 2, 5	s, 6; m(25), 6	a
24	J	b	ip	22.5	1.8	1.5, 1.5	2, 2, 3.5	s, 6; m(25), 6	a
25	J	b	ip	22.5	1.8	1.5, 1.5	2, 2, 5	s, 6; m(25), 6	a
26	J	b	ip	22.5	1.8	1.5, 1.5	2, 2, 5	s, 6; m(25), 6	a
27	J	b	ip	22.7	1.8	1.5, 1.5	2, 2, 5	m(25), 6	a
28	J	a	ip	22.7	1.8	1.5, 1.5	2, 2, 3.5	-	-
29	J	a	ip	22.7	1.8	1.5, 1.5	2, 2, 3.5	-	-
30	J	a	ip	22.7	1.8	1.5, 1.5	2, 2, 3.5	-	-
31	J	b	ip	22.7	1.8	1.5, 1.5	2, 4, 4	s, 6	a
32	J	a	ip	22.7	1.8	1.5, 1.5	2, 2, 3.5	-	-
33	J	b	ip	22.7	1.8	1.5, 1.5	2, 4, 4	m(25), 6	a
34	J	a	ip	22.7	1.8	1.5, 1.5	2, 2, 3.5	-	-
35	J	b	ip	22.7	1.8	1.5, 1.5	2, 4, 4	m(25), 6	a
36	J	b	ip	22.7	1.8	1.5, 1.5	2, 4, 4	s, 6	a
37	J	b	ip	22.7	1.8	1.5, 1.5	2, 2, 4	m(25), 6	a
38	J	b	ip	22.7	1.8	1.5, 1.5	2, 2, 3.5	s, 6	a
39	J	b	ip	22.7	1.8	1.5, 1.5	2, 2, 3.5	s, 6	a
40	J	b	ip	22.7	1.8	1.5, 1.5	2, 2, 3.5	s, 6	a
41	J	b	ip	22.7	1.8	1.5, 1.5	2, 2, 3.5	s, 6	a

42	J	b	ip	22.7	1.8	1.5, 1.5	2, 2, 3.5	s, 6	a
43	J	b	ip	22.7	1.8	1.5, 1.5	2, 2, 3.5	s, 6; m(25), 6	a
44	J	b	ip	22.7	1.8	1.5, 1.5	2, 2, 3.5	m(25), 6	a
45	J	b	ip	22.7	1.8	1.5, 1.5	2, 2, 3.5	m(25), 6	a
46	J	b	pp	15.2	1.8	-, 2	-, 2, -	m(10), 2	o
47	J	b	pp	15.2	1.8	-, 2	-, 2, -	m(10), 2	o
48	J	b	pp	15.2	1.8	-, 2	-, 2, -	m(10), 2	o
49	J	b	pp	15.2	1.8	-, 2	-, 2, -	m(10), 2	o
50	J	b	pp	15.2	1.8	-, 2	-, 2, -	m(10), 2	o
51	J	a	pp	15.2	1.5	2, 1.5	2, 2, -	-	-
52	J	a	pp	15.2	1.5	2, 1.5	2, 2, -	-	-
53	J	a	pp	15.2	1.5	2, 1.5	2, 2, -	-	-
54	L	a	ip	20	1	2.5, 2.5	3.5, 3.5, 3.5	-	-
55	L	a	ip	20	1	2.5, 2.5	3.5, 3.5, 3.5	-	-
56	L	a	ip	20	1	2.5, 2.5	3.5, 3.5, 3.5	-	-
57	L	a	ip	20	1	2.5, 2.5	3.5, 3.5, 3.5	-	-
58	L	a	ip	20	1	2.5, 2.5	3.5, 3.5, 3.5	-	-
59	L	a	ip	20	1	2.5, 2.5	3.5, 3.5, 3.5	-	-
60	L	a	ip	20	1	2.5, 2.5	3.5, 3.5, 3.5	-	-
61	L	a	ip	20	1	2.5, 2.5	3.5, 3.5, 3.5	-	-
62	L	a	ip	20	1	2.5, 2.5	3.5, 3.5, 3.5	-	-
63	L	a	ip	20	1	2.5, 2.5	3.5, 3.5, 3.5	-	-
64	L	a	pp	20	1	2.5, 2.5	3.5, 3.5, -	-	-
65	L	a	ip	20	1	2.5, 2.5	3.5, 3.5, 3.5	-	-
66	L	a	pp	20	1	2.5, 2.5	3.5, 3.5, -	-	-
67	L	a	ip	20	1	2.5, 2.5	3.5, 3.5, 3.5	-	-
68	L	a	pp	20	1	2.5, 2.5	3.5, 3.5, -	-	-
69	L	a	ip	20	1	2.5, 2.5	3.5, 3.5, 3.5	-	-
70	L	a	pp	20	1	2.5, 2.5	3.5, 3.5, -	-	-
71	L	b	pp	20	1	1.5, 1.5	2.5, 2.5, -	m(10), 2	g
72	L	b	pp	20	1	1.5, 1.5	2.5, 2.5, -	m(10), 2	g
73	L	b	pp	20	1	1.5, 1.5	2.5, 2.5, -	m(10), 2	g
74	L	b	pp	20	1	1.5, 1.5	2.5, 2.5, -	m(10), 2	g
75	L	b	pp	20	1	1.5, 1.5	2.5, 2.5, -	m(10), 2	g
76	L	b	ip	20	1	1.5, 1.5	2.5, 2.5, 3.5	m(10), 2	g
77	L	b	ip	20	1	1.5, 1.5	2.5, 2.5, 3.5	m(10), 2	g
78	L	b	ip	20	1	1.5, 1.5	2.5, 2.5, 3.5	m(10), 2	g
79	L	b	ip	20	1	1.5, 1.5	2.5, 2.5, 3.5	m(10), 2	g
80	L	b	ip	20	1	1.5, 1.5	2.5, 2.5, 3.5	m(10), 2	g
81	L	b	pp	20	1	1.5, 1.5	2.5, 2.5, -	m(10), 2	g
82	L	b	ip	20	1	1.5, 1.5	2.5, 2.5, 3.5	m(10), 2	g
83	L	b	pp	20	1	1.5, 1.5	2.5, 2.5, -	m(10), 2	g
84	L	b	ip	20	1	1.5, 1.5	2.5, 2.5, 3.5	m(10), 2	g
85	L	b	pp	20	1	1.5, 1.5	2.5, 2.5, -	m(10), 2	g
86	L	b	ip	20	1	1.5, 1.5	2.5, 2.5, 3.5	m(10), 2	g
87	L	b	pp	20	1	1.5, 1.5	2.5, 2.5, -	m(10), 2	g

S.2 Decoder specifics

For all sessions, the BCI decoders followed the form of Equation 1. On some sessions, the parameters M_1 and M_2 were derived from the standard Kalman filter. On other sessions, the parameters of M_1 and M_2 were derived from a modified version of the Kalman filter. We first describe the derivation from the standard Kalman filter. Using the data from the calibration block (described in Sections 2.5.1. – 2.5.3.), we fit the parameters of the Kalman filter using maximum-likelihood [1]. Then, we used those parameters to decode cursor kinematics from neural activity during closed-loop BCI control.

At each timestep, we first computed a one-step prediction $\hat{\mathbf{x}}_t^-$

$$\hat{\mathbf{x}}_t^- = A\hat{\mathbf{x}}_{t-1} + \mathbf{b} \tag{S1}$$

where $A \in \mathbb{R}^{r\times r}$, and $\mathbf{b} \in \mathbb{R}^{r\times 1}$. Then, the one-step prediction was updated using the neural activity $\mathbf{u}_t$ to obtain the cursor kinematics $\hat{\mathbf{x}}_t$

$$\hat{\mathbf{x}}_t = \hat{\mathbf{x}}_t^- + K(\mathbf{u}_t - C\hat{\mathbf{x}}_t^- - \mathbf{d}) \tag{S2}$$

where $C \in \mathbb{R}^{q\times r}$, and $\mathbf{d} \in \mathbb{R}^{q\times 1}$. The cursor kinematics $\hat{\mathbf{x}}_t$ was used to render the cursor on the screen. $K \in \mathbb{R}^{r\times q}$ is the Kalman gain [1] converged after many timesteps. Because the spike counts were z-scored, $\mathbf{d} = \mathbf{0}$, and because the kinematics were centered to the workspace, $\mathbf{b} = \mathbf{0}$. Combining equations S1 and S2 yields

$$M_1 = A - KCA \tag{S3}$$

$$M_2 = K \tag{S4}$$

Now we describe the modified Kalman filter used in some sessions [2]. We first reduced the dimensionality of the neural activity from the calibration block to a set of low-dimensional latent factors using factor analysis. At each timestep, we estimated the posterior mean of latent factors $\hat{\mathbf{z}}_t$.

$$\hat{\mathbf{z}}_t = \Lambda^T(\Lambda\Lambda^T + \Psi)^{-1}\mathbf{u}_t \tag{S5}$$

where $\mathbf{u}_t$ is defined as in Section 2.5., and $\mathbf{z} \in \mathbb{R}^{p\times 1}$ contains the p latent factors. The parameters $\Lambda \in \mathbb{R}^{q\times p}$ and $\Psi \in \mathbb{R}^{q\times q}$ were determined using the expectation-maximization algorithm [3]. Because $\mathbf{u}_t$ has a mean of $\mathbf{0}$ due to z-scoring, we do not need to explicitly subtract the mean in Equation S5. We related $\hat{\mathbf{z}}_t$ to the cursor kinematics to fit the Kalman filter parameters using the calibration data. This is in contrast to Equations S1 - S4, where the Kalman filter directly related the neural activity $\mathbf{u}_t$ to cursor kinematics. During closed-loop control, we used this modified Kalman filter which can be expressed in the form of Equation 1, where

$$M_2 = K\Lambda^T(\Lambda\Lambda^T + \Psi)^{-1} \tag{S6}$$

while M_1 remains the same (but the dimensionalities of the matrices K and C are now based on p rather than q). The specific decoding parameters (i.e., the kinematic elements in $\mathbf{x}_t$, whether standard or modified version of the Kalman filter was used, and the values of p and r) are defined for each session in Table S1.

S.3 Supplementary figures

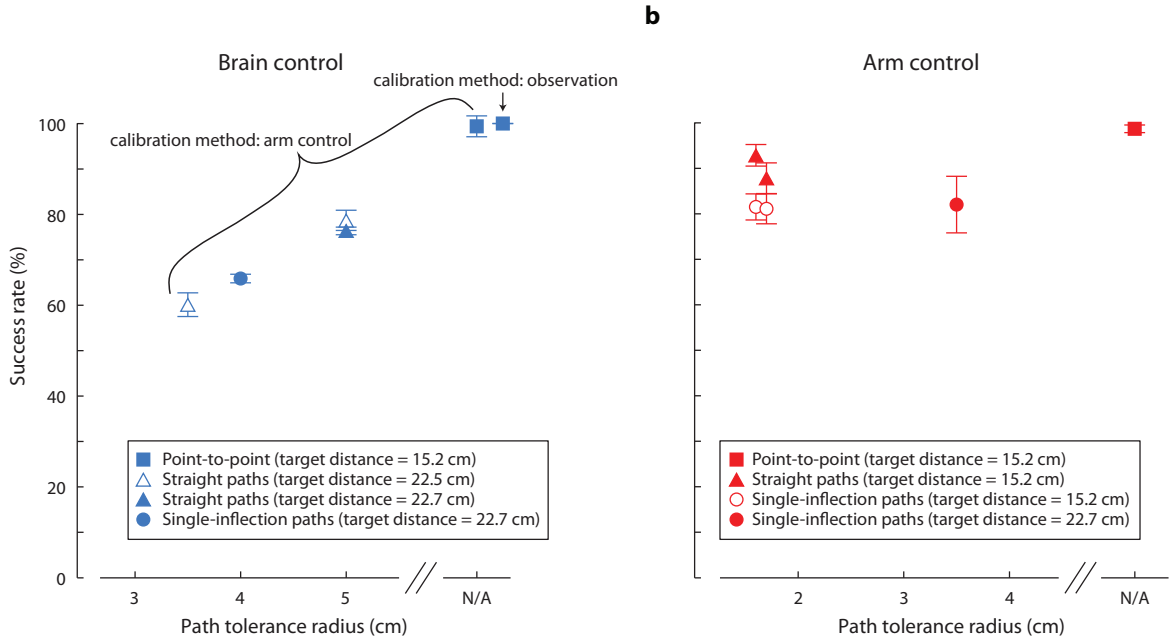

Figure S1: Success rates for monkey J. Success rates for monkey J are presented in a different format than monkey L since there were a variety of path tolerance radii and target distances for this monkey. Each data point represents the total success rate for trials from all sessions with the given task type, tolerance radius, and target distance. Error bars represent the 95% confidence interval based on the Bernoulli process. (a) Success rate versus instructed path tolerance radius for brain control. Success rates were larger as the tolerance radius increased, with the highest success rate for the point-to-point task. The success rates for straight paths with 5 cm tolerance radius were not significantly different from each other. All other brain control success rates are significantly different from each other. For a given tolerance radius, we would expect the success rate to be greater for the straight instructed paths than for the single-inflection instructed paths. Here, the single-inflection success rate is between the straight path success rates due to differences in tolerance radius. Point-to-point, arm control calibration: $n = 206$ trials; Point-to-point, observation calibration: $n = 8464$; Straight instructed paths, tolerance radius = 3.5 cm: $n = 1353$; Straight instructed paths, tolerance radius = 5 cm, target distance = 22.5 cm, $n = 8760$; Straight instructed paths, tolerance radius = 5 cm, target distance = 22.7 cm, $n = 1066$; Single-inflection instructed paths: $n = 9605$. (b) Success rate versus instructed path tolerance radius for arm control. Success rates were similar for all three task types. We believe this similarity was due to monkey J being motivated to perform better by the increased difficulty of the instructed path task. Point-to-point: $n = 4491$ trials; Straight instructed paths, tolerance radius = 1.6 cm: $n = 713$; Straight instructed paths, tolerance radius = 1.7 cm: $n = 505$; Single-inflection instructed paths, tolerance radius = 1.6 cm: $n = 810$; Single-inflection instructed paths, tolerance radius = 1.7 cm: $n = 622$; Single-inflection instructed paths, tolerance radius = 3.5 cm: $n = 168$. All arm control single-inflection instructed path success rates are not significantly different from each other. Arm control success rate with straight instructed path and tolerance radius 1.7 cm was not significantly different from arm control success rate with single-inflection instructed path and tolerance radius 3.5 cm. All other arm control success rate comparisons were significantly different.

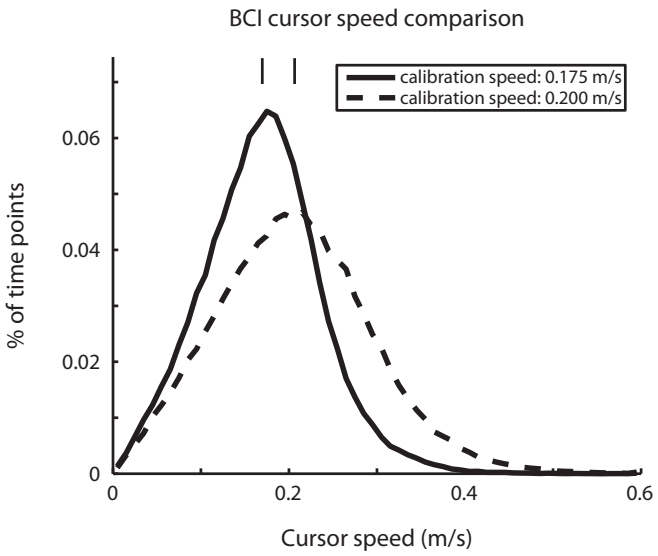

Figure S2: Calibration speed affects closed-loop BCI cursor speed. For monkey L, the BCI decoders analyzed in the main figures were calibrated with an observed cursor speed of 0.175 m/s. For other decoders (not analyzed in the main figures), we calibrated with an observed cursor speed of 0.20 m/s. The histograms show the closed-loop cursor speeds for each type of decoder. Vertical tick marks indicate the means of the distributions. The closed-loop speeds were significantly larger for the decoder calibrated with the larger observed cursor speeds ($p < 0.05$, Wilcoxon rank-sum test). Calibration speed = 0.175 m/s: n = 137,422 timesteps; Calibration speed = 0.200 m/s: n = 162,121 timesteps.

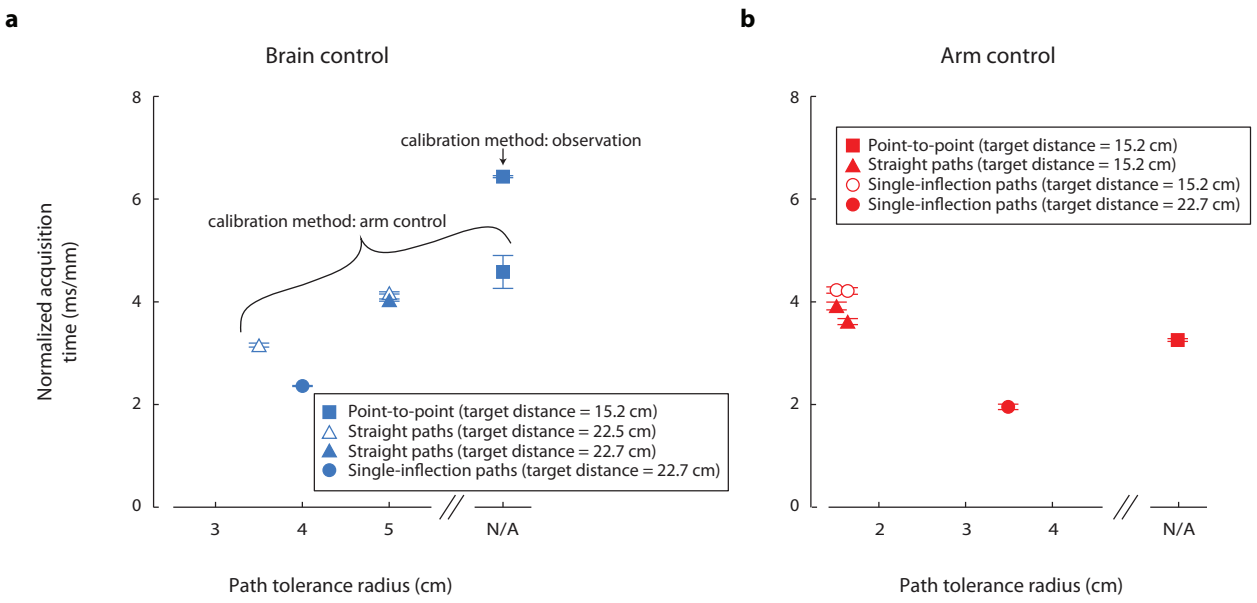

Figure S3: Normalized acquisition times for monkey J. Each data point represents the average normalized acquisition time for successful trials from all sessions with the given task type, tolerance radius, and distance between start and end target. Error bars represent mean +/- standard error. (a) Brain control normalized acquisition times. Normalized acquisition times for straight instructed path (target distance = 22.5 cm) and straight instructed path (target distance = 22.7 cm) are not statistically different ($p < 0.05$, Wilcoxon rank-sum test). All other comparisons are significantly different. For the point-to-point task under brain control, monkey J had a shorter normalized acquisition time when the decoder was calibrated using the arm control instructed-path task than when it was calibrated using observation. This difference may be due to the specific parameters of the observation task. If we had increased the speed of the cursor that the monkey observed, then the monkey likely would have been able to move the cursor faster (Figure S2). Point-to-point, arm control calibration: $n = 206$ successful trials; Point-to-point, observation calibration: $n = 8417$; Straight instructed paths, tolerance radius = 3.5 cm, target distance = 22.5 cm: $n = 813$; Straight instructed paths, tolerance radius = 5 cm, target distance = 22.5 cm: $n = 6690$; Straight instructed paths, tolerance radius = 5 cm, target distance = 22.7 cm: $n = 839$; Single-inflection instructed paths: $n = 6631$. (b) Arm control normalized acquisition times. Similar to monkey L, normalized acquisition times increase as task difficulty increases for a given target distance (point-to-point < straight instructed paths < single-inflection instructed paths). Normalized acquisition time decreased for single-inflection paths as the target distance and tolerance radius increased. All normalized acquisition time comparisons were significantly different ($p < 0.05$, Wilcoxon rank-sum test) except for straight instructed paths (radius = 1.6 cm) and straight instructed paths (radius = 1.7 cm). Point-to-point: $n = 4087$ successful trials; Straight instructed paths, tolerance radius = 1.6 cm: $n = 628$; Straight instructed paths, tolerance radius = 1.7 cm: $n = 478$; Straight instructed paths, tolerance radius = 3.5 cm: $n = 131$; Single-inflection instructed paths, tolerance radius = 1.6 cm: $n = 629$; Single-inflection instructed paths, tolerance radius = 1.7 cm: $n = 412$.

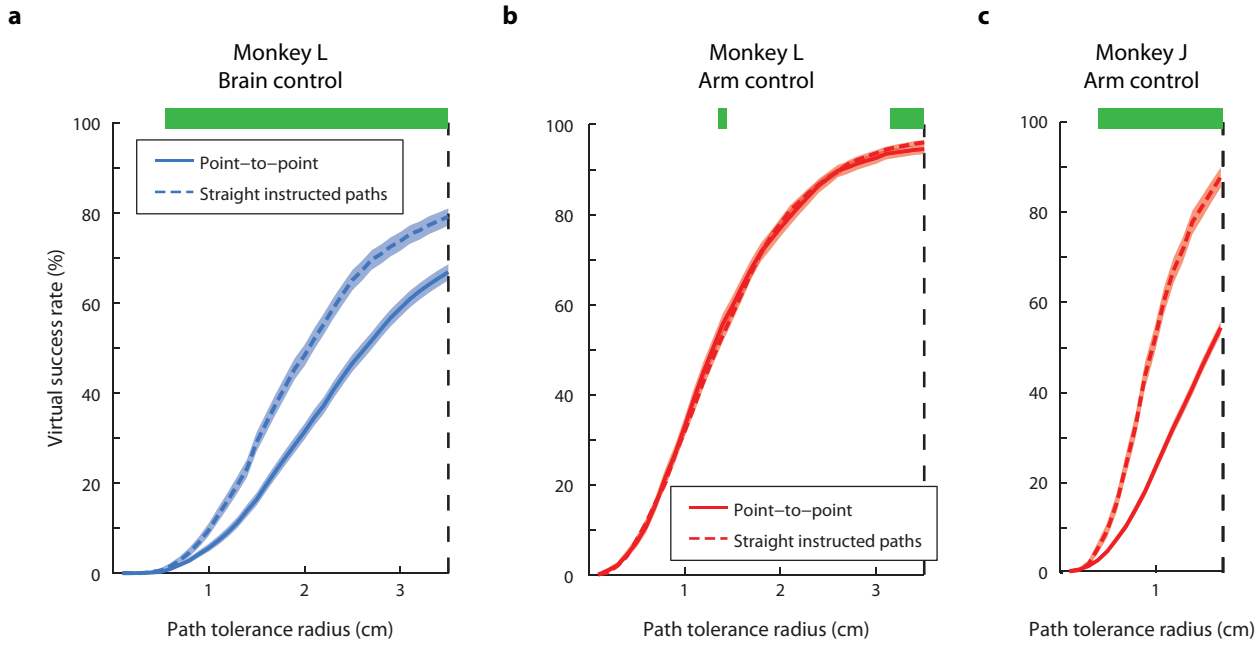

Figure S4: Virtual success rates across a wide range of virtual path tolerance radii. (a) Virtual success rates monkey L brain control. Solid lines are the mean virtual success rates, and the band is the 95% confidence interval based on the Bernoulli process. Dashed line is the tolerance radius that was applied online. Green bar, tolerance radii for which the virtual success rate for straight instructed path trials was significantly different than that for point-to-point trials. Target-to-target distance: 20 cm. Brain-control point-to-point, $n = 2660$ trials; Brain control straight instructed paths, $n = 1723$. (b) Virtual success rates for monkey L arm control. Same plotting format as a. Target-to-target distance: 20 cm. Arm control point-to-point, $n = 1859$; Arm control straight instructed paths, $n = 4259$. (c) Virtual success rates for monkey J arm control. Same plotting format as a. Point-to-point, $n = 4603$ trials; Straight instructed paths, $n = 713$.

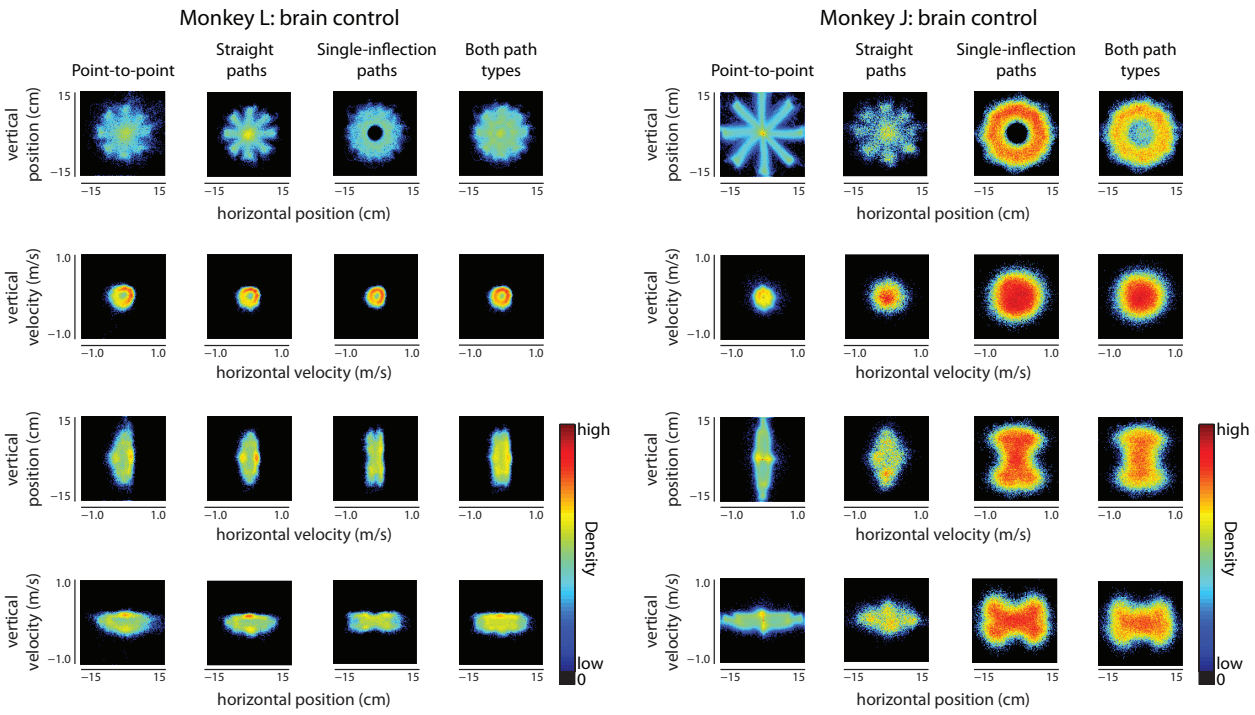

Figure S5: Kinematic histograms for different task types for monkey L (left) and monkey J (right) brain control. Same plotting format as Figure 9 (which shows kinematic histograms for arm control). The data from monkey J are from the same subset of sessions shown in Figure 5b.

References

[1] Wei Wu, Yun Gao, Elie Bienenstock, John P. Donoghue, and Michael J. Black. Bayesian population decoding of motor cortical activity using a Kalman filter. *Neural Comput.*, 18(1):80–118, January 2006.

[2] Patrick T Sadtler, Kristin M Quick, Matthew D Golub, Steven M Chase, Stephen I Ryu, Elizabeth C Tyler-Kabara, Byron M Yu, and Aaron P Batista. Neural constraints on learning. *Nature*, 512:423–426, 2014.

[3] A P Dempster, N M Laird, and D B Rubin. Maximum Likelihood from Incomplete Data via the EM Algorithm. *J. R. Stat. Soc.*, 39:1 – 38, 1977.